Normal Vibrations of β Brass

G. GILAT* AND G. DOLLING
Chalk River Nuclear Laboratories, Atomic Energy of Canada Limited, Chalk River, Ontario, Canada
(Received 8 October 1964; revised manuscript received 7 January 1965)

The normal modes of vibration of the ordered alloy of copper and zinc, β brass, have been extensively studied at 296°K by means of the coherent one-phonon scattering of slow neutrons from single-crystal specimens. The frequencies of normal modes propagating along the high-symmetry directions [00ζ], [ζζ0], [ζζζ], and [½½ζ] have been measured by means of a triple-axis crystal spectrometer for two specimens mounted in different orientations. These results may be satisfactorily described in terms of a restricted Born–von Kármán model (4*E*) with interatomic forces extending out to fourth-nearest-neighbor atoms, although Fourier analysis of sums of squares of certain normal-mode frequencies (taken in pairs) indicates the probable existence of nonzero forces extending at least to seventh neighbors. A feature of interatomic-force models for β brass is the large difference between the second-nearest-neighbor Cu-Cu and Zn-Zn forces. The experimental evidence does not, however, permit an unambiguous determination of which force is to be identified as Cu-Cu and which as Zn-Zn. A fairly successful attempt has been made to interpret the results in terms of more physically realistic models, in which the effective long-range forces are represented by an oscillatory potential arising from the mild singularity in the dielectric function at the Fermi level. The precise form of the coefficient of the oscillatory potential has been chosen on an empirical basis. Model 4E has been used as an interpolation formula for computing the frequency distribution function and its moments, and also the heat capacity of β brass. A selection of normal modes has been studied at several temperatures above 296°K, particularly in the vicinity of the order-disorder phase transition at about 727°K. The over-all structure of the dispersion curves appears to be substantially unchanged in the disordered phase, although certain "splittings" observed at 296°K become blurred into apparently continuous bands of frequencies at elevated temperatures. In all cases, the frequencies decrease and energy widths increase as the temperature increases. Two particular longitudinal-optic modes display a sharp increase in energy width at the transition temperature, in contrast to the generally smooth behavior of the other modes. No satisfactory explanation of these effects has yet been found.

1. INTRODUCTION

A CONSIDERABLE body of information concerning the thermal vibrations of solids has been accumulated in recent years; much of this information has been obtained for simple solids (i.e., having a simple structure, usually one atom per unit cell) by means of the coherent inelastic scattering[1] of slow neutrons. The present paper describes the application of these neutron-scattering techniques to the case of β brass, an alloy of copper and zinc in approximately equal proportions. Preliminary reports[2,3] of some of this work have already appeared. Earlier studies of the thermal vibrations of β brass have been made by Cole and Warren,[4] who determined certain normal-mode frequencies from x-ray diffuse-scattering measurements. Their results are in poor agreement with the present work, the frequencies being generally too low, by a factor of 2 in the worst case. Shibuya *et al.*[5] have calculated the dispersion relation for β brass using a simple Born–von Kármán force model (deduced from elastic-constant values) in which only the mass difference between Cu and Zn is taken into account. Their results show some similarities to analogous calculations to be described in Sec. 3.

At room temperature, β brass has an ordered CsCl structure, that is to say, it consists of two interpenetrating simple cubic lattices (lattice constant a), with the copper and zinc ions occupying positions (0,0,0) and $(\frac{1}{2},\frac{1}{2},\frac{1}{2})a$, respectively. As the temperature is increased, a transition of the second (or higher) degree to a simple bcc structure occurs; the transition temperature T_c is composition-dependent, being about 727°K for the specimen used in the high-temperature experiments described in Sec. 5. The neutron-scattering experiments have been performed at various temperatures, above and below T_c, to study the behavior of the thermal vibrations as a function of the degree of order.

When a beam of thermal neutrons is incident upon a crystalline solid, coherent-scattering processes may occur in which one phonon of the normal modes of vibration of the solid is created or destroyed with consequent changes in energy and momentum of the scattered neutrons. If the energy and momentum of the incident and scattered neutrons are E_0, $\hbar\mathbf{k}_0$ and E', $\hbar\mathbf{k}'$, respectively, the conditions governing these coherent one-phonon processes may be written

$$E_0-E'=\pm h\nu, \tag{1}$$

$$\mathbf{k}_0-\mathbf{k}'=\mathbf{Q}=2\pi\boldsymbol{\tau}+\mathbf{q}, \tag{2}$$

where ν is the frequency of the normal mode whose reduced wave vector is $\mathbf{q}$; $\mathbf{Q}$ is the momentum-transfer vector; and $\boldsymbol{\tau}$ is a vector of the reciprocal lattice of the crystal. Equations (1) and (2) are satisfied only when ν and $\mathbf{q}$ satisfy the "dispersion relation" for the normal

* N.R.C. Post-doctoral Fellow; Present address: Oak Ridge National Laboratory, Oak Ridge, Tennessee.

[1] G. Placzek and L. Van Hove, Phys. Rev. **93**, 1207 (1954).
[2] G. Gilat and G. Dolling, Bull. Am. Phys. Soc. **9**, 82 (1964).
[3] G. Dolling and G. Gilat, Solid State Commun. **2**, 79 (1964).
[4] H. Cole and B. E. Warren, J. Appl. Phys. **23**, 335 (1951).
[5] Y. Shibuya, Y. Fukuda, and T. Fukuroi, Sci. Rept. Res. Inst. Tôhoku Univ. Ser. A: **3**, 1 (1951).

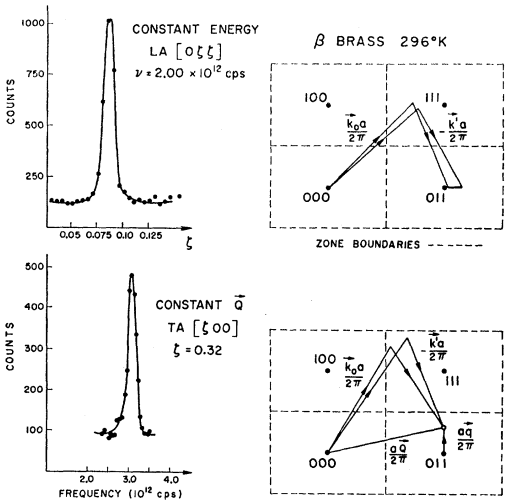

FIG. 1. Reciprocal-lattice diagrams illustrating typical constant-**Q** and constant-energy measurements together with the appropriate observed neutron groups.

modes of the material,

$$\nu = \nu_j(\mathbf{q}), \tag{3}$$

where j denotes the polarization of the normal mode. If the coherent one-phonon scattering processes can be observed and distinguished from all other possible scattering processes which may occur, the dispersion relation (3) is readily deduced by application of Eqs. (1) and (2) to the measured neutron energies and momenta. The nuclear properties of both copper and zinc are quite favorable for this purpose, and indeed neutron-scattering experiments on these elements (separately) have already been performed.[6–9]

The derivation of Eqs. (1) and (2) involves the assumption of *harmonic* interatomic forces within the solid by which the neutrons are scattered. If *anharmonic* effects are present, the δ functions of Eqs. (1) and (2) become broadened into approximately Lorentzian shapes and there is no longer a clear-cut distinction between one-phonon and multiphonon scattering processes. This subject has recently received considerable theoretical and experimental study.[10–12] The situation is further complicated in the case of β brass by the existence of defects arising from the departure from the ideal-ordered CsCl structure, which the present (nonstoichiometric) specimens display even at very low temperatures.

Of the many possible types of spectrometer with which inelastic-neutron-scattering measurements may be performed, one of the most convenient is the triple-axis crystal spectrometer.[13] All the experiments described in this paper were performed on the triple-axis spectrometer installed at the NRU reactor Chalk River.

2. EXPERIMENTS AT 296°K

Most of the measurements, including all those made at elevated temperatures (see Sec. 5), were made with a cylindrical specimen (I) having the following characteristics: composition 47 at.% Zn, length 2 in., diam. $\frac{3}{4}$ in., $[1\bar{1}1]$ axis parallel to the cylinder axis. Specimen I was oriented so that a $(1\bar{1}0)$-type mirror plane of the crystal was parallel to the incident and scattered neutron beams of the triple-axis spectrometer. A second cylindrical specimen (II) was employed in a small number of additional experiments at 296°K: composition 48 at.% Zn, length 2 in., diam. $\frac{3}{4}$ in., [001] axis parallel to the cylinder axis. Specimen II was oriented so that a (001)-type mirror plane of the crystal was parallel to the incident and scattered neutron beams. The mosaic spread of both specimens was approximately $\frac{1}{2}°$.

The experiments were carried out under conditions of either (a) constant momentum transfer of the neutron ("Constant **Q**" method[13]) or (b) constant energy transfer of the neutron.[13] Both methods are illustrated in Fig. 1. In the upper diagram, the energy transferred from neutron to crystal is kept constant while the momentum-transfer vector **Q** describes a straight line in reciprocal space. In the lower diagram, **Q** remains constant while the energy transfer is varied. In both examples, the scattered-neutron energy is kept constant, and in all the measurements only neutron-energy-loss processes were employed. The results for both crystal specimens at 296°K, are shown in Fig. 2. Constant **Q** (constant energy) measurements are plotted with vertical (horizontal) error bars where these exceed the size of the points.

Certain normal modes, e.g., all those propagating along the $[00\zeta]$ direction, and the longitudinal (L) modes propagating along $[\zeta\zeta 0]$, could be observed in the experiments on both specimens, and provide a test of the effect of small changes in composition. Within the experimental errors (1 to 2%), no significant discrepancies between the two crystals were observed, and hence no distinction according to specimen has been made in plotting the results in Fig. 2. Other normal modes were observable only on one or the other of the specimens. For example, the $T_1[\zeta\zeta 0]$ modes (i.e., with polarization vectors parallel to [001]) and all modes along $[\frac{1}{2}\frac{1}{2}\zeta]$ were measured using specimen I, while

[6] C. Cribier, B. Jacrot, and D. Saint-James, in *Inelastic Scattering of Neutrons in Solids and Liquids* (International Atomic Energy Agency, Vienna, 1961), p. 549.
[7] S. K. Sinha and G. L. Squires, J. Phys. Chem. Solids (to be published).
[8] G. Borgonovi, G. Caglioti, and J. J. Antal, Phys. Rev. **132**, 683 (1963).
[9] E. Maliszewski, J. H. Rosolowski, and D. Sledziewska, J. Phys. Chem. Solids (to be published).
[10] A. A. Maradudin and A. E. Fein, Phys. Rev. **128**, 2589 (1962).
[11] R. A. Cowley, *Advances in Physics* (Francis & Taylor, Ltd., London, 1963), Vol. 12, p. 421.
[12] B. N. Brockhouse, T. Arase, G. Caglioti, M. Sakamoto, R. N. Sinclair, and A. D. B. Woods, in *Inelastic Scattering of Neutrons in Solids and Liquids* (International Atomic Energy Agency, Vienna, 1961), p. 531.
[13] B. N. Brockhouse, in *Inelastic Scattering of Neutrons in Solids and Liquids* (International Atomic Energy Agency, Vienna, 1961), p. 113.

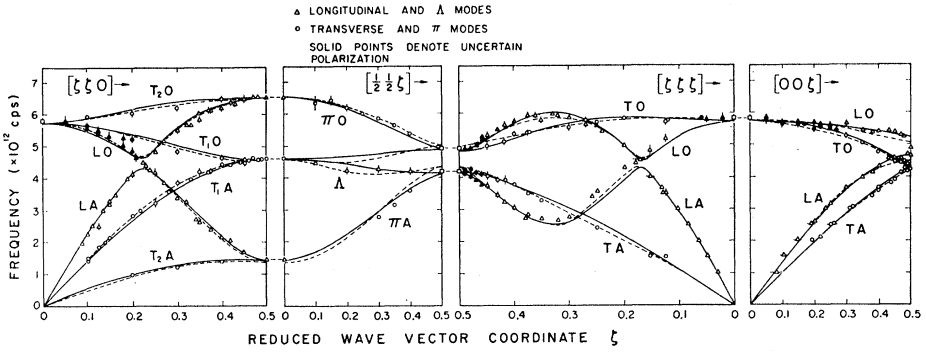

FIG. 2. Dispersion curves of β brass at 296°K for four high-symmetry directions. Triangular points denote L and Λ modes, and circles indicate T and π modes. Solid points denote uncertain polarization. The solid curve represents the Born–von Kármán fourth-nearest-neighbor model ($4E$) best fit. The dashed curve is the fit obtained with model (a) of Sec. 4, in which the oscillatory potential V_P is employed.

the $T_2[\zeta\zeta 0]$ modes (i.e., with polarization vectors parallel to $[1\bar{1}0]$) were observed using specimen II. The limiting slopes at zero wave vector of the acoustic-mode dispersion curves correspond to the appropriate sound velocities, which may be calculated from the 296°K elastic constants determined by McManus.[14] The elastic constants display a significant composition dependence,[14] but over the range 45 to 48 at.% Zn, the maximum variation is only about 2%. It is therefore not surprising that no significant differences in phonon frequencies were detected in our experiments with the two specimens. Further discussion of this point is given in Sec. 3.

The over-all shapes of the dispersion curves in Fig. 2 are rather similar to those which would be expected for a simple bcc material such as sodium, except that certain degeneracies are removed, by reason of the differences between copper and zinc. Only two of the theoretically expected "splittings" are large enough to be observable in the present experiments, namely, at $a\mathbf{q}/2\pi=(0.5,0.5,0.5)$ and for the longitudinal (L) modes at $a\mathbf{q}/2\pi=(0,0,0.5)$. Figure 3 shows two pairs of well-resolved neutron groups observed in constant-$\mathbf{Q}$ measurements carried out near $a\mathbf{Q}/2\pi=(1.5,1.5,0.5)$, i.e., near the zone boundary in the Λ direction. The magnitude of this splitting depends mainly on the difference between the second-nearest-neighbor copper-copper and zinc-zinc interatomic forces (see Sec. 3). The temperature dependence of this splitting is briefly mentioned in Sec. 5.

Throughout these measurements, the most suitable values of $\mathbf{Q}$ to choose for studying each normal mode $(\mathbf{q},j)$ were selected with the help of structure-factor[15] values computed from Born–von Kármán models of the interatomic forces in β brass. These models, and some computed structure-factor curves, are described in Sec. 3. The scattering lengths[16] for copper and zinc required for these calculations, together with other

TABLE I. Some properties of β brass.

			Reference
Lattice constant at 300°K		2.945 Å	
Debye temperature:			
(i) measured		284°K	23
(ii) calculated		281°K	This paper
Elastic constants at 300°K			14
(for 50 at.% Zn)	C_{11}	13.36×10^{11} dyn/cm²	
	C_{12}	10.38×10^{11} dyn/cm²	
	C_{44}	7.34×10^{11} dyn/cm²	
Mean scattering lengths:	Zn	0.59×10^{-12} cm	16
	Cu	0.77×10^{-12} cm	16
Composition: specimen	I	47 at.% Zn	
	II	48 at.% Zn	

[14] G. M. McManus, Phys. Rev. **129**, 2004 (1963).

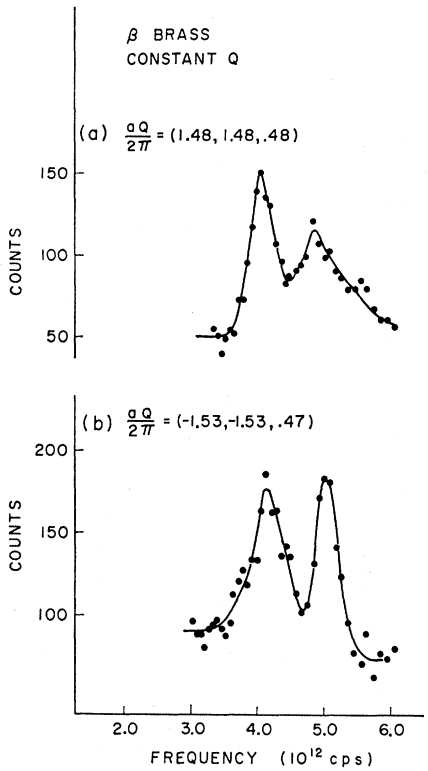

FIG. 3. Neutron groups associated with modes (a) $L[\zeta\zeta\zeta]$ and (b) $T[\zeta\zeta\zeta]$, near the Brillouin-zone boundary. A splitting into optic and acoustic branches is observed in both cases.

[15] B. N. Brockhouse and P. K. Iyengar, Phys. Rev. **111**, 747 (1958).

[16] D. J. Hughes and R. B. Schwartz, Brookhaven National Laboratory Report No. BNL-325, 1958 (unpublished).

relevant information concerning β brass, are given in Table I.

3. BORN–VON KÁRMÁN THEORY

In this section we describe the application of the Born–von Kármán theory to the ordered β-brass structure, the calculation of the frequency distribution function $g(\nu)$ for the normal modes and related thermodynamic quantities, and the calculation of the "reduced structure factors" which dominate the behavior of the coherent one-phonon scattering cross section as a function of $\mathbf{Q}$. No allowance has been made in these calculations for the slight departure from perfect order displayed by our specimens even at 296°K. A discussion of somewhat less phenomenological force models for β brass is given in Sec. 4.

Since there are two atoms in the primitive unit cell of perfectly ordered β brass (of stoichiometric composition), and since equilibrium positions of both atoms are at centers of inversion symmetry, the thermal vibrations may be expressed by means of a real, symmetric (6×6) matrix whose eigenvalues are proportional to the squares of the normal-mode frequencies. The matrix elements, which are linear functions of the interatomic force constants, are listed in Appendix A; details of the force-constant notation used, and of the conditions under which the dynamical matrix may be factorized, are also given in this Appendix. The 1st, 4th, 7th$\cdots$ nearest neighbors of an origin atom of type A are of type B, whereas the remaining neighbors (2nd, 3rd, 5th, 6th$\cdots$) are of the same type A. Thus force constants representing interactions between identical atoms are of two kinds, Cu-Cu and Zn-Zn. Extension of the Born–von Kármán theory to distant neighbors therefore involves a substantial number of disposable parameters. For example, a first-through-fifth-nearest-neighbor model (general forces) involves 20 force constants (cf. 13 constants for the simple bcc structure). Preliminary attempts to fit the experimental dispersion curves with such general force models (by means of a nonlinear least-squares-fitting program) showed (i) that forces only out to third- or fourth-nearest neighbors were important and (ii) that "tangential" or "shearing-type" force constants were always small or zero except for the first-nearest neighbor. A simple Fourier analysis may also be performed on the sums of the squared frequencies of various pairs of branches of the dispersion relation, e.g., the longitudinal-acoustic (LA) $[\zeta\zeta 0]$ and longitudinal-optic (LO)$[\zeta\zeta 0]$ branches. The Fourier coefficients are linear combinations of interatomic force constants, and the number of such coefficients required to obtain a good fit gives an indication of the *range* of the interatomic forces. Analysis of the results for β brass in this way shows that significant forces exist at least out to fifth, and very probably out at least to seventh, nearest neighbors. The fifth- through seventh-neighbor force constants are, however, relatively small, as indicated by the above mentioned Born–von Kármán analysis.

TABLE II. Best-fit values of interatomic force constants including fourth-nearest neighbors (Model 4E). (Only nonzero coefficients are listed).

Neighbor	Force constants (dyn/cm)	
1	$\alpha_1{}^1=8420$	$\beta_1{}^1=11\,340$
2	$\alpha_{10}{}^2=7110$	$\alpha_{11}{}^2=\ 730$
3	$\alpha_{10}{}^3=1070$	$\alpha_{11}{}^3=\ 1190$
4	$\alpha_1{}^4=\ 280$	$\beta_3{}^4=\ 370$

Accordingly, various restricted third- and fourth-neighbor Born–von Kármán force models were tried in order to obtain the best possible fit with the least number of disposable parameters. Tangential force constants such as $\alpha_{2\sigma}{}^2$, $\alpha_{3\sigma}{}^3$, and $\alpha_2{}^4$ were arbitrarily set to zero in most of the models considered. The final calculations were made by fitting the various force models (having, say, n_p disposable parameters) to 86 independent experimental data D_i, viz., 3 elastic constants[14] and the squared values of 83 phonon frequencies spaced regularly along all the branches shown in Fig. 2. If the computed values of these 86 quantities are labeled C_i, then the quality of fit for any particular model is conveniently expressed by the ratio

$$F=\sum_i (C_i-D_i)^2 W_i/(86-n_p)\,, \tag{4}$$

where W_i are weighting factors given by the experimental errors of the D_i. A satisfactory fit is obtained when F is of order 1. For the most general second-neighbor model ($n_p=6$) $F=9.16$, while the best third-neighbor model ($a_{2\sigma}{}^2=\alpha_{3\sigma}{}^3=0$, $n_p=8$) gave $F=3.11$. When certain fourth-neighbor constants ($\alpha_1{}^4$ and $\beta_2{}^4$) were added and $\beta_{3\sigma}{}^3$ put equal to zero, however, a quite satisfactory fit was finally obtained ($n_p=8$, $F=1.38$). This fourth-neighbor fit is shown as the solid curves in Fig. 2. Values of the force constants used in computing the solid curves are listed in Table II. We shall refer to this model as 4E. A general feature of all these calculations was that almost identical fits could be achieved for any model merely by interchanging the masses M_0 and M_1, or alternatively, by labeling all the Cu-Cu force constants as Zn-Zn type, and vice versa. Reference to Table II shows that, for example, $\alpha_{10}{}^2 \gg \alpha_{11}{}^2$: However, it is impossible to determine unambiguously from these best-fit computations which constant refers to Cu and which to Zn. Although it is probable that this question may be settled only by means of a theoretical calculation of these force constants from first principles, some experimental indication of the correct labeling is given by the neutron group intensities observed for the $\Lambda[\frac{1}{2}\frac{1}{2}\zeta]$ modes which correspond to independent vibrations of Cu and Zn atoms. With the help of eigenvectors for various normal modes, obtained from a suitable force model, the neutron group intensities arising from

coherent one-phonon scattering[15,17] involving those modes may be estimated. The scattered-neutron intensity is sensitively dependent upon the so-called "inelastic structure factor," given by

$$g_j^2 = |\sum_\sigma \mathbf{Q}\cdot\xi_{\sigma j} b_\sigma \exp(2\pi i \boldsymbol{\tau}\cdot\mathbf{r}_\sigma)|^2, \quad (5)$$

where $\xi_{\sigma j}$ is the eigenvector appropriate to the σ atom in the unit cell (j denotes the mode), b_σ and $\mathbf{r}_\sigma$ are the scattering length and position with respect to the cell origin of the σ atom, and $\boldsymbol{\tau}$ is defined by Eq. (2). (We here ignore the small differences between the Debye-Waller factors and masses of Cu and Zn.) For the directions of high symmetry shown in Fig. 2, ξ_{0j} and ξ_{1j} have a common *direction*, denoted by a unit vector ξ_j. A "reduced structure factor" can then be defined by

$$g_j^2 = |b_0 \mathbf{Q}\cdot\xi_j|^2 f_j^2, \quad (6)$$

where, if $\mathbf{r}_0$ is taken to be 0,

$$f_j^2 = |\xi_0 + (b_1/b_0)\xi_1 \exp(2\pi i \boldsymbol{\tau}\cdot\mathbf{r}_1)|^2. \quad (7)$$

Figure 4 shows curves of f_j^2 against ζ for the high-symmetry directions, computed from model 4*E* described in Table II.

If we consider the above mentioned $\Lambda[\frac{1}{2}\frac{1}{2}\zeta]$ modes, it is clear that scattered-neutron energy distributions at appropriate values of $\mathbf{Q}$ should in principle consist of two peaks, associated with independent vibrations of the Cu and Zn sublattices, respectively. The former peak should be more intense, and its identification would permit the correct assignment of the *AA*- and *BB*-type force constants. The frequencies of the two Λ modes are, however, very similar for all ζ (see Fig. 2) and no well-resolved neutron groups were obtained in experiments designed to observe them. The shapes of the peaks observed did suggest that the lower frequency mode is probably associated with the copper atom vibrations, i.e., that the Cu-Cu second-neighbor constant is the smaller one. However, this conclusion is largely tentative at the present time.

Some remarks should perhaps be made at this point concerning the elastic constants of β brass, and the extent to which they are fitted by the force model 4*E*. As mentioned in Sec. 2, there is a significant composition dependence of the elastic constants at 296°K. The calculated values of elastic constants obtained in the least-squares-fitting analyses tended towards the values appropriate to a specimen of the ideal stoichiometric composition. The neutron measurements refer to normal modes whose wavelengths are 10 to 15 interatomic distances at most, whereas the sound velocity measurements utilize wavelengths of order 10^2 times longer than this. The short wavelength phonons are perhaps well-defined within regions of perfectly ordered crystal, and their frequencies may then be expected to refer to the ideal structure rather than to the composition of macroscopic regions of the specimen.

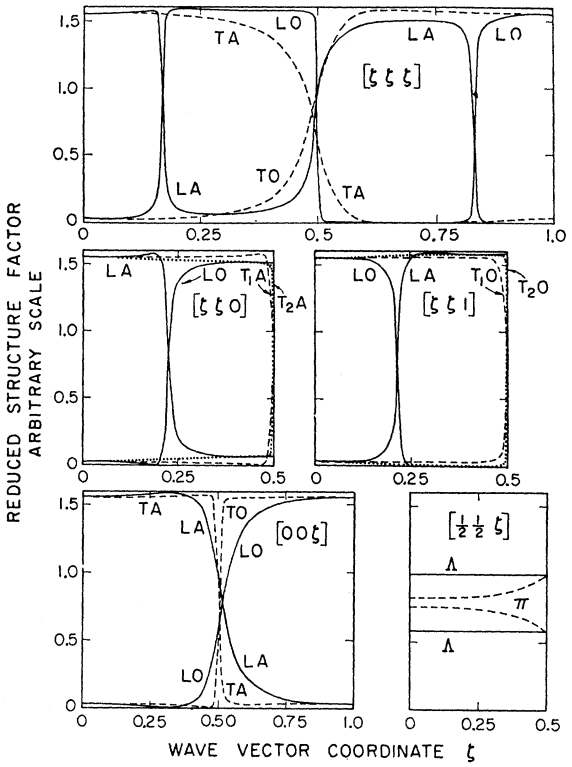

FIG. 4. The reduced structure factor calculated from model 4*E* for all the high-symmetry directions in β brass. Solid lines represent the reduced structure factor for *L* or Λ modes, dashed lines for *T*, T_1, or π modes. The dotted lines along the $[\zeta\zeta 0]$ and $[\zeta\zeta 1]$ directions represent the T_2 modes.

The Born–von Kármán models described above are of course purely phenomenological, and several arbitrary restrictions have been imposed upon the force constants. However, these models may well be adequate as interpolation formulas for calculating normal mode frequencies which have not been experimentally measured. We believe that model 4*E* is quite satisfactory for this purpose, and hence also for computing the frequency distribution function $g(\nu)$ and related thermodynamic properties of β brass. The problem of constructing less arbitrary force models will be discussed in Sec. 4.

Methods for calculating the distribution function $g(\nu)$ for the normal modes of vibration of a crystal have been discussed at length by Maradudin *et al.*[18] These methods require initial data, which may consist of certain branches of $\nu_j(\mathbf{q})$ from which frequencies of "critical points"[19] may be deduced, or of a given interatomic force model which fits that dispersion relation. The most straightforward method of calculating $g(\nu)$ is the sampling method, in which a large number of pho-

[17] I. Waller and P. O. Fröman, Arkiv Fizik 4, 183 (1952).

[18] A. A. Maradudin, E. W. Montroll, and G. H. Weiss, *Solid State Physics*, edited by F. Seitz and D. Turnbull (Academic Press Inc., New York, 1963), Suppl. 3, p. 1.

[19] L. Van Hove, Phys. Rev. 89, 1189 (1953).

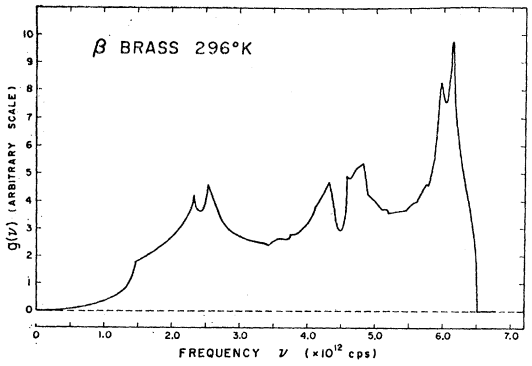

FIG. 5. The frequency distribution function for β brass obtained from model $4E$ by means of extrapolation method (Ref. 20). In this histogram, the frequencies of 96 018 048 normal vibrations are sorted into over 300 channels of width $\Delta\nu=0.02\times10^{12}$ cps. (For further details see Appendix B.)

non frequencies, corresponding to a uniform distribution of wave vectors throughout the Brillouin zone, are computed in some way (usually by means of a force model). These are sorted into appropriate frequency intervals $\nu\rightarrow\nu+\Delta\nu$ and the results presented in histogram form. The chief objection to this method is that calculation of phonon frequencies by matrix diagonalization is very laborious, and this so severely restricts the number of calculated frequencies that only very crude histograms of $g(\nu)$ can be obtained. This difficulty has been largely overcome by means of an extrapolation method developed by the present authors.[20] The normal mode frequencies corresponding to a relatively small number of wave vectors $\mathbf{q}_c$, distributed uniformly through the irreducible segment of the Brillouin zone (1/48 in the case of β brass), are calculated by matrix diagonalization. Each $\mathbf{q}_c$ is at a corner of a simple cubic mesh, chosen so that points of high symmetry in reciprocal space [e.g., (000), (100), etc.] lie at the body centers of cubes of the mesh. [The alternative choice, with (000) at a corner of a cube, is less efficient, and leads to difficulties concerning degenerate modes.] Surrounding each "crude mesh point" $\mathbf{q}_c$ a large number of closely and uniformly spaced wave vectors (on a "fine" mesh) are chosen. The normal mode frequencies for these points are obtained by linear extrapolation from $\mathbf{q}_c$. The frequency gradients required for this extrapolation are obtained with the help of standard perturbation methods. Details of the application of this technique to β brass are given in Appendix B. The resulting frequency distribution function $g(\nu)$ is illustrated in Fig. 5. Figure 5 is, in fact, a histogram plot of $g(\nu)\Delta\nu$, but the individual points and their fluctuations (of the order of 1%) are too small to be shown separately. All the expected critical points show up quite clearly, and the distribution is more than adequate for the purpose of calculating thermodynamic properties on the basis of model $4E$. Frequency distribution functions for β brass have previously been calculated,[4,21] for example, by the method of Houston.[22] Although a similar number of prominent peaks appears in one[21] of these earlier distributions, their relative intensities and spacings are quite different from those shown in Fig. 5. A conventional presentation of the calculated lattice heat capacity of β brass, by way of the variation of Debye temperature θ_D with temperature, is given in Fig. 6. The low-temperature limit $\theta_D(0°\text{K})=281°$ is in good agreement with that obtained from low-temperature heat capacity[23] and elastic-constant[14] measurements. It should be emphasized that all of these calculations are based on a harmonic-force model appropriate to 296°K, and that no corrections have been made for the variation of normal-mode frequencies with temperature. Thus the calculated $\theta_D(T)$ curve is expected to be between 5 and 10°K too low at very low temperatures. A potentially more useful method of presenting these results is to calculate the moments M_n of $g(\nu)$:

$$M_n=\int_0^\infty \nu^n g(\nu)d\nu \Big/ \int_0^\infty g(\nu)d\nu. \tag{8}$$

Since the numerical values of M_n span a very wide range, it is convenient to define[24] a Debye spectrum of "cut-off" frequency ν_n, having the same moment M_n as the calculated spectrum:

$$\nu_n=\left[\frac{n+3}{3}\int_0^\infty \nu^n g(\nu)d\nu \Big/ \int_0^\infty g(\nu)d\nu\right]^{1/n} \quad \text{for } n\neq0, n>-3. \tag{9}$$

For $n=0$, -3, we have

$$\nu_0=\exp\left[1/3+\int_0^\infty (\ln\nu)g(\nu)d\nu \Big/ \int_0^\infty g(\nu)d\nu\right], \tag{10}$$

$$\nu_{-3}=(k_B/h)\theta_D, \quad (T=0°\text{K}),$$

where k_B is the Boltzmann constant.

The advantages of this method of presentation have been described by Barron *et al.*[24] The necessary analysis of heat-capacity data to obtain values of ν_n for β brass has not yet been performed, and so only values calculated from model $4E$ are shown in Fig. 7. A detailed comparison of experimental and theoretical moment curves will require extensive heat-capacity measurements.

[20] G. Gilat and G. Dolling, Phys. Letters **8**, 304 (1964). The $g(\nu)$ for β brass mentioned in that paper is based on an earlier force model, fitted to a smaller number of experimental results than are utilized in the present calculations.

[21] Y. Shibuya, Y. Fukuda, and T. Fukuroi, Sci. Rept. Res. Inst. Tôhoku Univ. Ser. A: **3**, 182 (1951).

[22] W. V. Houston, Rev. Mod. Phys. **20**, 161 (1948).

[23] B. W. Veal and J. A. Rayne, Phys. Rev. **128**, 551 (1962).

[24] T. H. K. Barron, W. T. Berg, and J. A. Morrison, Proc. Roy. Soc. (London) **A242**, 478 (1957).

4. THE EFFECTIVE INTERATOMIC POTENTIAL

Attempts have recently been made to calculate from first principles an "effective" interatomic potential function (and hence the interatomic forces) for a number of metals, for example, Na,[25–27] Cu,[28] and also Zn.[29] A division is made of the total potential into three contributions: (i) the very short-range "overlap" potential V_{BM} between immediate neighbors, (ii) the long-range Coulomb potential V_C between the bare ions, and (iii) the potential V_E arising from the interaction through the conduction electrons, including the electron-electron interaction. Contributions (ii) and (iii) are rather large, and, owing to the screening effect of the conduction electrons, tend to cancel each other out for increasing range. The overlap potential (i) is usually treated empirically, for example, by means of an exponential (Born-Mayer) form with adjustable parameters. The bare-ion contribution (ii) may readily be calculated by standard methods, while (iii) can, under certain assumptions, be expressed in terms of a "form factor" and "dielectric function" for the metal.

A fairly satisfactory description of the observed $\nu_j(\mathbf{q})$ for both Na [25–27] and Cu [28] has been obtained with this kind of model, and in spite of certain difficulties (e.g., the selection of suitable numerical values for the term V_{BM}), it seems possible that the problem of β brass may be approached from this viewpoint. We adopt, however, a different approach. Since the interatomic potential (in real space) at short range is quite complicated, a separation is made into two parts (i) interactions extending to first- and second-neighbor atoms and (ii) long-range interactions for third-nearest neighbors and beyond. Two distinct descriptions, I and II,

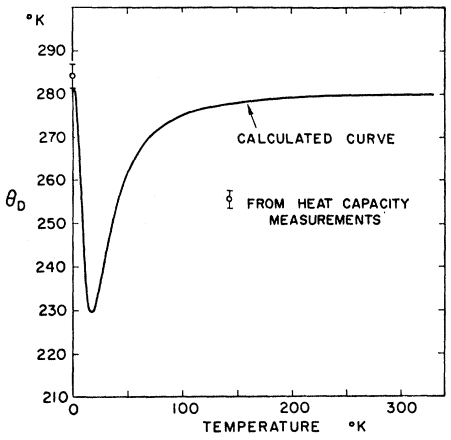

FIG. 6. The Debye temperature (θ_D) as a function of temperature, calculated on the basis of the force model 4E. No corrections have been made for the temperature dependence of the normal-mode frequencies.

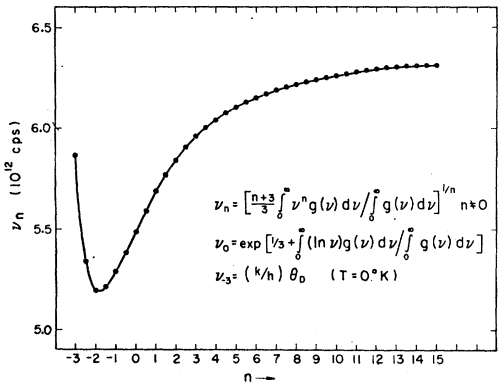

FIG. 7. The Debye "cutoff" frequency ν_n as a function of n, obtained from the moments of the distribution function (Fig. 5).

have been employed for the short-range interactions. In I, we assume that the potential consists of a Born-Mayer term V_{BM} responsible for repulsive forces between first neighbors and between second-neighbor Cu-Cu atoms, together with a small screened electrostatic potential of the Thomas-Fermi form

$$V_{SE}=(Z_j/r_{ij})e^{-k_s r_{ij}}, \tag{11}$$

where Z_j is an "effective charge" on the jth ion, r_{ij} is the distance between ions i and j, and k_s is related to the Fermi radius k_F and the Bohr radius of the hydrogen atom a_H by

$$k_s^2=4k_F/\pi a_H. \tag{12}$$

This expression for V_{SE} is a poor approximation at short range, but since its contribution is very small compared to V_{BM}, its precise form is of little practical significance. In the second description II we avoid any assumptions concerning the nature of the potentials by replacing $(V_{BM}+V_{SE})$ by four empirical Born–von Kármán force constants α_1^1, β_1^1, α_{10}^2, and α_{11}^2. The second-neighbor "tangential" force constants α_{20}^2 and α_{21}^2 are neglected, as in model 4E (Sec. 3).

For the long-range part of the interatomic interaction, we assume an oscillatory potential V_P of the form

$$V_P(r_{ij})\sim(1/r_{ij})^3\cos(2k_F r_{ij}+\phi), \tag{13}$$

where ϕ is an adjustable phase angle. This oscillatory potential originates from the mild singularity[30] in the dielectric function $\epsilon(Q)$ of the metal for $Q=2k_F$. An oscillatory term of this kind has been derived for the case of an impurity ion embedded in a host metal,[31–33] and also by Koenig[34] who used the Born approximation

[25] T. Toya, J. Res. Inst. Catalysis, Hokkaido Univ. **6**, 183 (1958).
[26] W. Cochran, Proc. Roy. Soc. (London) **A276**, 308 (1963).
[27] L. J. Sham, Proc. Roy. Soc. (London) **A283**, 33 (1965).
[28] T. Toya, Progr. Theoret. Phys. (Kyoto) **20**, 974 (1958).
[29] W. A. Harrison, Phys. Rev. **129**, 2512 (1963).
[30] J. Bardeen, Phys. Rev. **52**, 689 (1937).
[31] J. Friedel, Nuovo Cimento, Suppl. **7**, 287 (1958).
[32] J. S. Langer and S. H. Vosko, J. Phys. Chem. Solids **12**, 196 (1959).
[33] A. Blandin and J. L. Déplanté, *Metallic Solid Solutions*, edited by J. Friedel and A. Guinier (W. A. Benjamin Inc., New York, 1963), Paper IV, p. 1.
[34] S. H. Koenig, Phys. Rev. **135**, A1693 (1964). (We are grateful to Dr. Koenig for sending us a preprint.)

TABLE III. Numerical results of best-fit calculations for models involving the long-range oscillatory potential V_P: (a) short-range forces described by $(V_{BM}+V_{SE})$, and "shearing" forces neglected; (b) same as (a) but with shearing forces included; (d) range forces described by four Born–von Kármán parameters, again neglecting shearing forces. Set (c) is results obtained by other authors, denoted by superscripts. Set (e) is model 4E parameters for comparison (see Table II).

Set	W_0 eV	W' eV	ρ Å^{-1}	k_s Å^{-1}	A 10^6 erg-cm	B 10^6 erg-cm	ϕ rad	F
(a)	0.096	0.120	11.5	1.92	−2.14	−0.46	2.09	1.29
(b)	0.097	0.129	11.5	1.99	−1.98	−0.68	1.94	1.32
(c)		0.120[a]	11.5[a]	1.91			1.86[35]	
	$\alpha_1{}^1$	$\beta_1{}^1$	$\alpha_{10}{}^2$	$\alpha_{11}{}^2$ [b]				
(d)	8360	10 940	6890	290	−2.09	−0.47	2.08	1.30
(e)	8420	11 340	7110	730				

[a] Reference 28.
[b] Born–von Kármán force constants (dynes/cm).

to calculate the scattering of free electrons by planes of atomic dipoles in Na. Harrison and Paskin[35] used such a potential to calculate the order-disorder energy in β brass. For a simple metal such as Na, the expression (13) for V_P should be multiplied by a parameter A which depends on the screening charge distribution around an ion. The case of β brass is slightly complicated by the existence of two kinds of atom. Simple considerations based on a nearly-free electron model lead to parameters A_{00}, A_{11}, and $A_{10}=(A_{00}\cdot A_{11})^{1/2}$, representing the Cu-Cu, Zu-Zn, and Cu-Zn interactions, respectively. However, this form for the long-range part of the potential leads to a fit to the experimental results which is scarcely better than the fit obtained for a Born–von Kármán model involving first- and second-neighbor forces only.

It is perhaps not surprising that this simple approach is unsuccessful, since it is based on a single plane-wave approximation for the conduction electrons, implying that the off-diagonal terms of the (matrix) dielectric function ϵ are zero.[36] The Fermi surface of β brass intersects the first (simple cubic) Brillouin zone,[37] and even if it is still an acceptable approximation to assume a spherical Fermi surface, it is necessary to admix more plane waves in order to describe the conduction electrons satisfactorily. In the light of this consideration, the exact form of V_P remains unclear. A successful attempt has, however, been made to fit the experimental results with a semiempirical expression of the form

$$V_P(r_{ij})=(A'\pm B')(1/r_{ij})^3\cos(2k_Fr_{ij}+\phi), \quad (14)$$

where $A'=A_{00}'=A_{11}'=A_{10}'$ and B' is an additional term depending on the off-diagonal components of ϵ. The + sign refers to Cu-Cu and Zn-Zn interactions while the − sign is to be used for calculating the Cu-Zn interactions. The chief advantage of this expression is that (as will be discussed below) it provides a good description of the results with a fairly small number of disposable parameters. Clearly, it cannot be regarded as satisfactory in the absence of a rigorous derivation from a basic formalism such as is described in Ref. 36. It is interesting to note that the same expression Eq. (14) with A' set to zero was employed in the calculation[35] of the ordering energy.

Once an explicit form for the total effective potential has been chosen, it is relatively straightforward to calculate the potential energy W_{ij} associated with the interaction of pairs of atoms i, j, and hence the Born–von Kármán force constants from which the vibration frequencies can be computed in the usual manner. We consider the total potential to be of the form $(V_{BM}+V_{SE}+V_P)$, from which it will be clear how the calculations are performed when $(V_{BM}+V_{SE})$ is replaced by Born–von Kármán force constants. The interaction energy is given by

$$W_{ij}=W_0e^{-\rho(r-r_{01})}+W_0'e^{-\rho'(r-r_{01})}+(Z_iZ_j/r_{ij})e^{-k_sr_{ij}}+[(A''\pm B'')/(r_{ij})^3]\cos(2k_Fr_{ij}+\phi), \quad (15)$$

where r_{01} is the first-neighbor Cu-Zn distance. The first and second terms are the Born-Mayer core-repulsion potentials effective only between the first-nearest neighbors, and between second-nearest-neighbor Cu ions, respectively. The disposable parameters ρ and ρ' may be taken to be the same since the quality of fit is relatively insensitive to $(\rho-\rho')$. In the "Thomas-Fermi" term, we assume[35] the effective charges Z_i to be $+0.5e$ $(-0.5e)$ for Zn(Cu) ions, respectively. Since its contribution is in any case rather small, this somewhat arbitrary assumption is of small significance. In the final calculations, the value of k_F was taken to be 1.515 Å^{-1} (i.e., 0.710 reciprocal lattice units), appropriate to three conduction electrons per unit cell. (If k_F is treated as a free parameter, the "fitted" value does not differ appreciably from this value.)

We now express the interactions in terms of interatomic force constants, keeping only the dominant terms of each contribution. As mentioned earlier, the

[35] R. J. Harrison and A. Paskin, J. Phys. Radium **23**, 613 (1962). See also A. Paskin, Phys. Rev. **134**, A246 (1964).
[36] L. J. Sham and J. M. Ziman, Solid State Phys. **15**, 221 (1963). See in particular p. 270, Eq. (12.16), and p. 272, Eq. (13.4).
[37] J.-P. Jan, W. B. Pearson, and M. Springford, in Proceedings of the Ninth International Conference on Low Temperature Physics, Columbus, Ohio, 1964 (unpublished).

tangential constants, defined by

$$\Phi_{ij}{}^t=(1/r)(\partial W/\partial r)_{r=r_{ij}} \quad (16)$$

have been found to be small for all except first-nearest-neighbor ions. This fact is consistent with the approximations involved in deriving Eq. (13), viz., that terms of higher order than $(1/r_{ij})^3$ are neglected. In many of the calculations, therefore, we have made the simplifying assumption that $\Phi_{ij}{}^t=0$ (except for first neighbors). We present below the results of two nonlinear least-squares-fitting investigations (using the same 86 experimental results for β brass at 296°K as described in Sec. 3) in which this assumption is made. In the first model (a), the total effective potential is taken as $(V_{BM}+V_{SE}+V_P)$, while in the second model (d), we replace $(V_{BM}+V_{SE})$ by the four disposable forces constants $\alpha_1{}^1$, $\beta_1{}^1$, $\alpha_{10}{}^2$, and $\alpha_{11}{}^2$. To show that the effect of the above assumption is indeed small, we also present a recalculation of model (a), including the tangential force constants. This is called model (b). In all of these calculations, force constants extending out to 11th-nearest-neighbor ions were computed from the appropriate interaction energy. The results for the three models (a), (b), and (d) are given in Table III. Figure 2 shows (dashed curves) the best fit to the experimental results obtained with model (a), compared with the eight-parameter Born–von Kármán model 4E (solid curves) discussed in Sec. 3. A slightly better over-all fit to the results is obtained with model (a), which has seven disposable parameters, W_0, W_0', ρ, k_s, A, B, and ϕ. [A and B are very simply related to A'' and B'' in Eq. (15).] It is interesting to note that the Born–von Kármán parameters calculated in model (d) are in excellent agreement with those derived from model (a) (see Table IV), and also, except for $\alpha_{11}{}^2$, with those of model 4E. The value of k_s calculated from Eq. (12) is 1.91 Å^{-1}, approximately equal to the best-fit values obtained for models (a) and (b). Values for W_0' and ϕ, obtained by other authors, are also given in Table III.

TABLE IV. Interatomic force constants and phase factors calculated from model (a) (see Table III). Force constants not listed below may be derived either from symmetry or from the restrictive assumptions appropriate to model (a).

Neighbor	Position	Representative force constants dyn/cm	$(2k_Fr+\phi)/\pi$
1	(111)	$\alpha_1{}^1=$ 8280	
		$\beta_1{}^1=$10 990	3.125
2	(200)	$\alpha_{10}{}^2=$ 7160	3.505
		$\alpha_{11}{}^2=$ 360	
3	(220)	$\alpha_1{}^3=$ 710	4.682
4	(311)	$\alpha_1{}^4=$ 320	5.375
5	(222)	$\alpha_1{}^5=$ −120	5.585
6	(400)	$\alpha_1{}^6=$ −430	6.346
7	(331)	$\alpha_1{}^7=$ 200	6.855
8	(420)	$\alpha_1{}^8=$ 520	7.016
9	(422)	$\alpha_1{}^9=$ −120	7.622
10–11	(333)	$\alpha_1{}^{10}=$ −90	8.044
	(511)	$\alpha_1{}^{11}=$ −250	8.044

TABLE V. Temperature dependence of frequency and linewidth for 7 normal modes in β brass.

Wave vector ($a\mathbf{Q}/2\pi$) mode	Temperature °K	Frequency (10^{12} cps)	Linewidth[a] (10^{12} cps)
(1.30,1.30,1.0)	296	3.39±0.04	0.50
LA Σ	499	3.27±0.05	0.44
	693	3.23±0.05	0.70
	714	3.22±0.06	0.80
	725	3.21±0.08	0.80
	739	3.22±0.10	0.85
	751	3.17±0.09	0.70
	774	3.12±0.15	1.00
(1.0,1.0,0.37)	296	3.44±0.04	0.25
TA Δ	693	3.16±0.04	0.40
	714	3.15±0.05	0.50
	739	3.11±0.05	0.50
	774	3.07±0.05	0.55
(1.0,1.0,0.32)	296	3.06±0.03	0.20
TA Δ	499	2.96±0.04	0.30
	693	2.81±0.03	0.38
	714	2.77±0.03	0.40
	739	2.76±0.04	0.40
	751	2.73±0.04	0.50
	774	2.71±0.04	0.45
(1.20,1.20,0.20)	296	4.99±0.05	0.24
LO Δ	499	4.90±0.07	0.42
	693	4.80±0.06	0.65
	714	4.73±0.05	0.55
	739	4.73±0.08	0.90
	751	4.68±0.10	0.90
	774	4.71±0.07	0.90
(1.18,1.18,0.0)	296	3.82±0.04	0.24
LA Σ	693	3.65±0.04	0.40
	714	3.63±0.04	0.45
	739	3.62±0.04	0.40
	774	3.59±0.05	0.40
(1.27,1.27,0.0)	296	5.20±0.05	0.35
LO Σ	499	5.09±0.07	0.50
	693	5.00±0.06	0.55
	714	5.01±0.06	0.55
	739	4.90±0.08	0.85
	751	4.91±0.12	0.80
	774	4.94±0.06	0.90
(1.13,1.13,0.13)	360	3.65±0.04	0.30
LA Δ	714	3.42±0.04	0.45
	739	3.41±0.05	0.55

[a] Errors are in most cases of the order of 20%.

5. MEASUREMENTS AT HIGH TEMPERATURES

Two series of measurements have been made in which the energies and energy widths of selected normal modes of vibration have been measured at several temperatures, both above and below the order-disorder transition temperature T_c. A general result of these measurements is that the normal-mode energies decrease and the widths increase as the temperature T rises. It is of particular interest to compare and correlate the behavior of various normal modes, and to attempt to detect any anomalous temperature effects as T passes through T_c. An account of the first series of measurements has already been given,[3] in which no definite conclusions were drawn concerning either correlations between modes or anomalous energy shifts or widths near T_c. For certain longitudinal modes, however, there were indications of possible anomalous increases in width of the observed scattered neutron groups, and a second series of more precise measure-

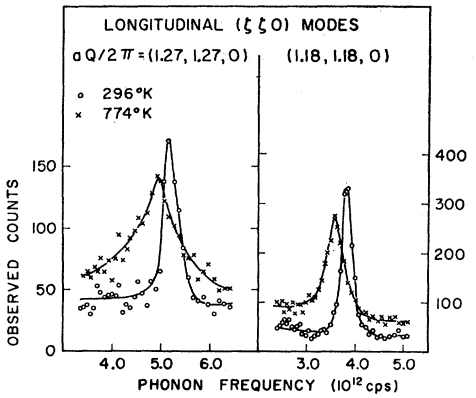

FIG. 8. Observed neutron groups associated with two different modes of the same polarization $L[\zeta\zeta 0]$, each at two different temperatures (below and above T_c). The frequency shifts as well as the changes in width are clearly shown. The change in the width is noticeably larger for the $\zeta=0.27$ mode.

ments was carried out to investigate these possibilities in further detail. An apparently significant correlation was then observed between the character of certain normal modes and the behavior, as a function of temperature, of the energy width of the associated neutron groups. The results of both sets of measurements are mutually consistant and are discussed together below.

The energies and energy widths of seven normal modes specially selected for the sharpness and high intensity of the associated scattered neutron groups, were measured at several temperatures both above and below the transition temperature T_c, and the results are listed in Table V. The system for labeling the normal modes in Table V differs from that used in the earlier account[3] where the modes were assigned labels "optic" (O) or "acoustic" (A) according to the kind of atomic motions involved (i.e., according to the *eigenvectors*). This convention is experimentally convenient but leads to ambiguities in the regions of "splitting" between longitudinal (L) modes near $a\mathbf{q}/2\pi=(0.22,0.22,0)$ and $(0.17,0.17,0.17)$ (we refer to these wave vectors as $\mathbf{q}_{S1}$ and $\mathbf{q}_{S2}$). We now define the optic mode in each case to be that with the *higher* frequency, and disregard the change in *character* (i.e., the phase relation between the Cu and Zn atoms) of the L modes which occurs near the wave vectors $\mathbf{q}_{S1}$ and $\mathbf{q}_{S2}$.

For most normal modes studied, the energy and energy width vary smoothly with temperature even through the transition point. All the energies decrease and widths increase with increasing temperature. Thus, although the scattered neutron groups associated with the mode $LA\Sigma(1.30,1.30,1.0)$ are at each temperature much wider than those of $LA\Sigma(1.18,1.18,0.0)$, in both cases a smooth variation of width is observed. The behavior of the mode $LO\Sigma(1.27,1.27,0.0)$ is, on the other hand, significantly different; a sharp increase in width is observed when the temperature is raised through T_c. The observed neutron groups for two of these modes at two temperatures, are illustrated in Fig. 8. A similar effect is observed for the mode $LO\Lambda$ $(1.20,1.20,0.20)$. Only these two normal modes, of all those studied, display other than smooth monotonic behavior as a function of temperature. In both cases, the wave vector is somewhat greater than that of the closest approach of the LO and LA branches ($\mathbf{q}_{S1}$ and $\mathbf{q}_{S2}$). The observed frequency widths for these modes are illustrated in Fig. 9, together with sketches of the relevant parts of reciprocal space and the wave vector values. A typical transverse-acoustic mode is included for comparison. It shows no anomalous behavior near T_c. The normal-mode frequencies in all cases show a smooth decrease with temperature, within the accuracy of the present measurements. In this connection, it is interesting to note the anomalous temperature dependence[14] of the elastic constant C_{44} in the vicinity of T_c.

It would perhaps be too daring to draw any definite conclusions concerning the anomalous behavior of L modes on the basis of these two examples. It would be highly desirable to obtain more experimental data before such conclusions are drawn. However, the experimental conditions under which such observations may be made at all are quite restrictive, and so we cannot readily produce further independent examples of similar anomalies. Assuming, nevertheless, that these energy-width anomalies are indeed real, it seems plausible that they are closely associated with the type of mode involved, and perhaps also with its wave vector and/or frequency. It is interesting to point out (though this

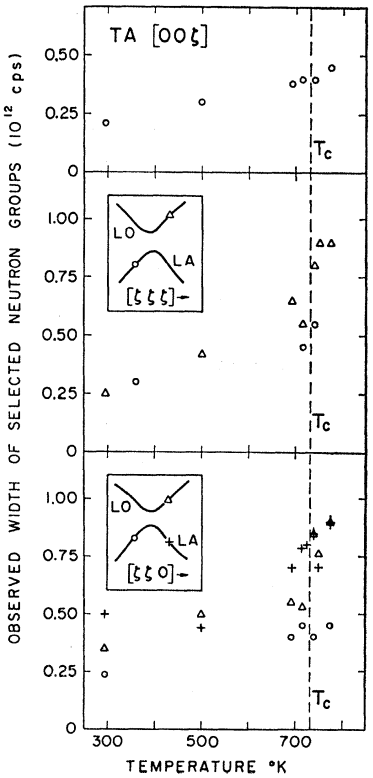

FIG. 9. The observed frequency width, as a function of temperature, is plotted for several phonons. The location of these phonons on the dispersion curves is schematically shown. For the transverse-acoustic (TA) mode, $\zeta=0.32$. The variation of linewidth in the vicinity of T_c for the longitudinal-optic (LO) mode (triangles) differs qualitatively from that of the other modes studied.

may be purely coincidental) that the magnitudes of $2\pi/\mathbf{q}_{S1}$ and $2\pi/\mathbf{q}_{S2}$ are similar, and are of the order of the extent of the short-range order ($\sim$10 Å) which is known[38] to exist in β brass at temperatures just above T_c. From another viewpoint, the contrast between the smooth temperature behavior of $T[00\zeta]$ modes and the possible anomalous behavior of certain longitudinal modes is not too surprising. An order-disorder transition will, presumably, influence mainly the $\alpha_{10}^2, \alpha_{11}^2$ force constants, which display the largest (and only significant) difference between the two kinds of atom. These force constants are absent from the expressions (see Appendix A) for the frequencies of the transverse modes mentioned. As yet, however, no reasonable framework has been established within which these anomalies may be completely understood.

It is of interest to mention the behavior of the "splitting" of the normal modes for wave vectors near (0.5,0.5,0.5) as a function of temperature. The two neutron groups are fairly well resolved at 296°K (see Fig. 3), but considerable blurring together has occurred even for $T=499$°K. Above this temperature, it was no longer possible to resolve the two peaks. One would expect to observe such a single wide peak for $T>T_c$; its appearance for $T<T_c$ may well be due to the poor instrumental focusing conditions prevailing in these particular experiments.

A few remarks should be made about the intensities of the observed neutron groups as a function of temperature. No attempt has been made to compare in detail the intensities at different temperatures. Such an analysis would be very inaccurate, particularly at the higher temperatures owing to the large increase in "background" intensity and to the relatively poor statistics in the wings of the distributions. These facts also contribute to the error in the measurement of the widths of the neutron groups. The precision of the width measurements (about 20% in most cases) is, however, substantially better than that of the intensities. In any event, no significant changes in the intensity of any of the neutron groups were observed in the vicinity of T_c.

6. CONCLUSIONS

A study of the normal mode vibration frequencies for ordered β brass at 296°K has revealed the existence of fairly long-range effective interatomic forces. The dispersion curves can be reasonably well described in terms of an entirely empirical Born–von Kármán model involving forces extending to fourth-nearest-neighbor ions, although Fourier analysis of the curves indicates the probable existence of at least seventh-neighbor forces. By setting a rather arbitrary selection of force constants to zero, the number of disposable parameters of this model ($4E$) is reduced to 8. While this model is probably adequate as an interpolation formula for computing vibration frequencies, the frequency distribution function, and various thermodynamic quantities (within the pseudoharmonic approximation), it lacks any physical justification in terms of real interatomic forces. A fairly successful attempt has been made to construct force models which, although still burdened with several disposable parameters, can be more closely correlated with the various kinds of force believed to exist in metal crystals. More theoretical work is needed, however, to justify the particular form of the oscillatory potential V_P employed in these calculations. A calculation from basic principles of the short-range part of the potential is also required.

Experiments at high temperatures, especially near the order-disorder transition temperature, have shown that the general features of the normal modes of vibration are retained even in the "disordered" phase. Certain "splittings" in the 296°K dispersion curves are, however, blurred out into apparently continuous bands of frequencies. The vibration frequencies and energy widths generally vary smoothly with temperature, but two examples have been found of anomalous increases in width, which are definitely associated with the order-disorder transition itself. No reasonable explanation of these effects has yet been found.

ACKNOWLEDGMENTS

We are indebted to Dr. R. A. Cowley, Dr. A. D. B. Woods, and Professor W. Cochran, F.R.S., for most valuable discussions, and to E. A. Glaser and A. L. Bell for technical assistance. We would also like to thank Dr. L. J. Sham, Professor W. Kohn, and Professor R. J. Elliott for the interest they have shown in this work. One of us (G.G.) wishes to express his appreciation of the hospitality he has enjoyed at Atomic Energy of Canada Ltd., and to thank the National Research Council for the award of a Fellowship.

APPENDIX A

The elements of the dynamical matrix for the β brass (CsCl) lattice may be written as four distinct expressions. The convention adopted here follows that of Squires,[39] who has given the two distinct expressions appropriate to monatomic bcc and fcc lattices. Let us define $\Phi_{nj}{}^{p\sigma}$ as the force acting on the origin atom in the ith direction when an atom "p" moves unit distance in the jth direction. $\sigma=0, 1$ stands for the two different atoms (Cu or Zn) which may be at the origin. The force constant matrix $\Phi^{p,\sigma}$ consists of elements $\alpha_{i\sigma}{}^s$ and $\beta_{i\sigma}{}^s$ in the following manner:

$$\begin{matrix} \alpha_{1\sigma}{}^s & \beta_{3\sigma}{}^s & \beta_{2\sigma}{}^s \\ \beta_{3\sigma}{}^s & \alpha_{2\sigma}{}^s & \beta_{1\sigma}{}^s \\ \beta_{2\sigma}{}^s & \beta_{1\sigma}{}^s & \alpha_{3\sigma}{}^s, \end{matrix} \tag{A1}$$

[38] C. B. Walker and D. T. Keating, Phys. Rev. **130**, 1726 (1963).

[39] G. L. Squires, *Inelastic Scattering of Neutrons in Solids and Liquids* (International Atomic Energy Agency, Vienna, 1963), Vol. II, p. 71.

where s is the order of the neighbor. Let $h_i{}^s$ denote (in units of half the cubic unit cell side) the equilibrium position of an sth-nearest neighbor, and n^s the number of such neighbors. In the case of a perfectly ordered CuZn lattice we have, for odd $h_i{}^s$,

$$\begin{aligned}\alpha_{i0}{}^s&=\alpha_{i1}{}^s,\\ \beta_{i0}{}^s&=\beta_{i1}{}^s,\end{aligned}\tag{A2}$$

and we shall drop the subscript σ in these cases. Then the four general expressions for the (6×6) dynamical matrix elements are:

$$\begin{aligned}
A_{i+3\sigma,i+3\sigma}&=(1/24\pi^2M_\sigma)\sum_s\epsilon_s n^s\sum_j\alpha_{j\sigma}{}^s\{2-C_{j,i}{}^s[C_{j+1,i+1}{}^sC_{j+2,i+2}{}^s+C_{j+2,i+1}{}^sC_{j+1,i+2}{}^s]\},\\
A_{i+3\sigma,k+3\sigma}&=(1/24\pi^2M_\sigma)\sum_s\epsilon_s n^s\sum_j\beta_{j\sigma}{}^sC_{j,i+2}[S_{j+1,i}{}^sS_{j+2,i+1}{}^s+S_{j+2,i}{}^sS_{j+1,i+1}{}^s],\\
A_{i+3,i}=A_{i,i+3}&=[1/24\pi^2(M_0M_1)^{1/2}]\sum_s(1-\epsilon_s)n^s\sum_j\alpha_j{}^s\{2-C_{j,i}{}^s[C_{j+1,i+1}{}^sC_{j+2,i+2}{}^s+C_{j+2,i+1}{}^sC_{j+1,i+2}{}^s]\},\\
A_{i+3,k}=A_{i,k+3}&=[1/24\pi^2(M_0M_1)^{1/2}]\sum_s(1-\epsilon_s)n^s\sum_j\beta_j{}^sC_{j,i+2}{}^s[S_{j+1,i}{}^sS_{j+2,i+1}{}^s+S_{j+2,i}{}^sS_{j+1,i+1}{}^s]\cdots,
\end{aligned}\tag{A3}$$

where:

$$\begin{aligned}C_{j,i}{}^s&=\cos\pi a h_j{}^s\zeta_i,\\ S_{j,i}{}^s&=\sin\pi a h_j{}^s\zeta_i,\\ \epsilon_s&=1\quad\text{for}\quad h_i{}^s\text{ even},\\ &=0\quad\text{for}\quad h_i{}^s\text{ odd},\end{aligned}$$

and M_σ is the mass of the σ-type atom (i.e., M_0 or M_1). The indices i, j, k can only take the values 1, 2, or 3. In the terms $C_{j,i}{}^s$, $S_{j,i}{}^s$, expressions such as $i+1$, $i+2$, which exceed 3, are to be interpreted as $i-2$, $i-1$, respectively. Similarly, the subscript k is taken to be $i+1$ unless $i=3$, when $k=1$. Since the matrix A is symmetric, permutation of indices in these four expressions yields all 36 elements. If μ, η are new indices taking the values 1, 2,⋯6, and $\delta_{\mu\eta}$ is the Kronecker delta symbol, then the secular equation yielding the squares of the normal-mode frequencies for a given wave vector $\mathbf{q}=(\zeta_1,\zeta_2,\zeta_3)(2\pi/a)$ is

$$|A_{\mu\eta}-\delta_{\mu\eta}\nu^2|=0.\tag{A4}$$

This equation can be factorized for wave vectors in directions of high symmetry in the reciprocal lattice, i.e., [00ζ], [$\zeta\zeta$0], [$\zeta\zeta\zeta$], and [$\frac{1}{2}\frac{1}{2}\zeta$]. For the first three directions, the squares of the frequency ν^2 are roots of a

TABLE VI. Combinations of force constants for modes propagating along directions of high symmetry.

Branch	GN[a]	$\Phi_n{}^\sigma$ $n=2$	$n=4$	$n=6$
[00ζ]L	Δ	$\alpha_{1\sigma}{}^2+4\alpha_{1\sigma}{}^3+4\alpha_{1\sigma}{}^5$	0	0
[00ζ]T	Δ	$\alpha_{2\sigma}{}^2+2\alpha_{1\sigma}{}^3+2\alpha_{3\sigma}{}^3+4\alpha_{1\sigma}{}^5$	0	0
[$\zeta\zeta\zeta$]L	Λ	$\alpha_{1\sigma}{}^2+2\alpha_{2\sigma}{}^2+3\alpha_{1\sigma}{}^5-2\beta_{1\sigma}{}^5$	$2\alpha_{1\sigma}{}^3+\alpha_{3\sigma}{}^3+2\beta_{3\sigma}{}^3$	$\alpha_{1\sigma}{}^5+2\beta_{1\sigma}{}^5$
[$\zeta\zeta\zeta$]T	Λ	$\alpha_{1\sigma}{}^2+2\alpha_{2\sigma}{}^2+3\alpha_{1\sigma}{}^5+\beta_{1\sigma}{}^5$	$2\alpha_{1\sigma}{}^3+\alpha_{3\sigma}{}^3-\beta_{3\sigma}{}^3$	$\alpha_{1\sigma}{}^5-\beta_{1\sigma}{}^5$
[$\frac{1}{2}\frac{1}{2}\zeta$]Λ		$\alpha_{1\sigma}{}^2-4\alpha_{1\sigma}{}^3+4\alpha_{1\sigma}{}^5$	0	0
[$\frac{1}{2}\frac{1}{2}\zeta$]$\pi$		$\alpha_{2\sigma}{}^2-2\alpha_{1\sigma}{}^3-2\alpha_{3\sigma}{}^3+4a_{1\sigma}{}^5$	0	0
[$\zeta\zeta$0]L	Σ	$\alpha_{1\sigma}{}^2+\alpha_{2\sigma}{}^2+2\alpha_{1\sigma}{}^3+2\alpha_{3\sigma}{}^3$	$\alpha_{1\sigma}{}^3+\beta_{3\sigma}{}^3+2\alpha_{1\sigma}{}^5+2\beta_{1\sigma}{}^5$	0
[$\zeta\zeta$0]T_1	Σ	$2\alpha_{2\sigma}{}^2+4\alpha_{1\sigma}{}^3$	$\alpha_{3\sigma}{}^3+2\alpha_{1\sigma}{}^5$	0
[$\zeta\zeta$0]T_2	Σ	$\alpha_{1\sigma}{}^2+\alpha_{2\sigma}{}^2+2\alpha_{1\sigma}{}^3+2\alpha_{3\sigma}{}^3$	$\alpha_{1\sigma}{}^3-\beta_{3\sigma}{}^3+2\alpha_{1\sigma}{}^5-2\beta_{1\sigma}{}^5$	0

Branch	Φ_n $n=1$	$n=3$	$n=5$
[00ζ]L	$4\alpha_1{}^1+8\alpha_2{}^4$	$4\alpha_1{}^4$	0
[00ζ]T	$4\alpha_1{}^1+4\alpha_1{}^4+4\alpha_2{}^4$	$4\alpha_2{}^4$	0
[$\zeta\zeta\zeta$]L	$3\alpha_1{}^1-2\beta_1{}^1+\alpha_1{}^4+2\alpha_2{}^4+2\beta_1{}^4-4\beta_2{}^4$	$\alpha_1{}^1+2\beta_1{}^1+2\alpha_1{}^4+4\alpha_2{}^4-4\beta_1{}^4$	$\alpha_1{}^4+2\alpha_2{}^4+2\beta_1{}^4+4\beta_2{}^4$
[$\zeta\zeta\zeta$]T	$3\alpha_1{}^1+\beta_1{}^1+\alpha_1{}^4+2\alpha_2{}^4-\beta_1{}^4+2\beta_2{}^4$	$\alpha_1{}^1-\beta_1{}^1+2\alpha_1{}^4+4\alpha_2{}^4+2\beta_1{}^4$	$\alpha_1{}^4+2\alpha_2{}^4-\beta_1{}^4-2\beta_2{}^4$
[$\frac{1}{2}\frac{1}{2}\zeta$]Λ	0	0	0
[$\frac{1}{2}\frac{1}{2}\zeta$]$\pi$	$-4\beta_1{}^1+8\beta_2{}^4$	$-4\beta_1{}^4$	0

Branch	$n=2$	$n=4$
[$\zeta\zeta$0]L	$2\alpha_1{}^1+2\beta_1{}^1+2\alpha_1{}^4+4\alpha_2{}^4+2\beta_1{}^4-4\beta_2{}^4$	$2\alpha_1{}^4+2\alpha_2{}^4+4\beta_2{}^4$
[$\zeta\zeta$0]T_1	$2\alpha_1{}^1+2\alpha_1{}^4+4\alpha_2{}^4$	$4\alpha_2{}^4$
[$\zeta\zeta$0]T_2	$2\alpha_1{}^1-2\beta_1{}^1+2\alpha_1{}^4+4\alpha_2{}^4-2\beta_1{}^4+4\beta_2{}^4$	$2\alpha_1{}^4+2\alpha_2{}^4-4\beta_2{}^4$

[a] Group-theoretical notation.

TABLE VII. Symmetry conditions for interatomic force constants.

Order of neighbor s	Position[a] of neighbor h_i^s	n_s	Type of force	Force-constant conditions	
1	(1,1,1)	8	AB	$\alpha_q{}^1=\alpha_2{}^1=\alpha_3{}^1$	$\beta_1{}^1=\beta_2{}^1=\beta_3{}^1$
2	(2,0,0)	6	AA or BB	$\alpha_{2\sigma}{}^2=\alpha_{3\sigma}{}^2$	$\beta_{1\sigma}{}^2=\beta_{2\sigma}{}^2=\beta_{3\sigma}{}^2=0$
3	(2,2,0)	12	AA or BB	$\alpha_{1\sigma}{}^3=\alpha_{2\sigma}{}^3$	$\beta_{1\sigma}{}^3=\beta_{2\sigma}{}^3=0$
4	(3,1,1)	24	AB	$\alpha_2{}^4=\alpha_3{}^4$	$\beta_2{}^4=\beta_3{}^4$
5	(2,2,2)	8	AA or BB	$\alpha_{1\sigma}{}^5=\alpha_{2\sigma}{}^5=\alpha_{3\sigma}{}^5$	$\beta_{1\sigma}{}^5=\beta_{2\sigma}{}^5=\beta_{3\sigma}{}^5$

[a] In units of $(a/2)$, where a is the cubic unit cell side.

quadratic equation, yielding the so-called acoustic (ν_A) and optic (ν_O) branches. The expressions for the frequencies can be written for these cases in the general form

$$\nu_{O,A}{}^2=(1/4\pi^2M_0M_1)\{M_0L_1+M_1L_0 \pm[(M_{01}L-M_1L_0)^2+4M_0M_1L^2]^{1/2}\}, \quad \text{(A5)}$$

where L_σ and L have the following forms

$$L_\sigma=R+\sum\Phi_n{}^\sigma(1-\cos\pi n\zeta), \qquad L=-R+\sum\Phi_n(1-\cos\pi n\zeta). \quad \text{(A6)}$$

R, $\Phi_n{}^\sigma$, and Φ_n are linear combinations of force constants. R is given by

$$R=4\alpha_1{}^1+4\alpha_1{}^4+8\alpha_2{}^4+\cdots, \quad \text{(A7)}$$

while $\Phi_n{}^\sigma$ and Φ_n are listed in Table VI.

Factorization of the matrix for the fourth direction $[\frac{1}{2}\frac{1}{2}\zeta]$ yields two modes (Λ and π) each of which is separated into two distinct branches. The solutions are

$$\nu_{\Lambda,\sigma}{}^2=(1/2\pi^2M_\sigma)[R+K_\sigma+\sum\Phi_n{}^\sigma(1-\cos\pi n\zeta)], \quad \text{(A8)}$$

$$\nu_{O,A}{}^2=(1/4\pi^2M_0M_1)\{M_0B_1+M_1B_0 \pm[(M_0B_1-M_1B_0)^2+4M_0M_1B^2]^{1/2}\}, \quad \text{(A9)}$$

where B_σ and B are given by

$$B_\sigma=R+C_\sigma+\sum\Phi_n{}^\sigma(1-\cos\pi n\zeta), \qquad B=C+\sum\Phi_n(1-\cos\pi n\zeta). \quad \text{(A10)}$$

K_σ, C_σ, and C are linear combinations of force constants, whose explicit expressions, for the first- through fifth-nearest neighbors, are

$$K_\sigma=4\alpha_{2\sigma}{}^2+8\alpha_{1\sigma}{}^3, \quad \text{(A11)}$$

$$C_\sigma=2\alpha_{1\sigma}{}^2+2\alpha_{2\sigma}{}^2+4\alpha_{1\sigma}{}^3+4\alpha_{2\sigma}{}^3, \quad \text{(A12)}$$

$$C=4\beta_1{}^1-8\beta_2{}^4+4\beta_1{}^4. \quad \text{(A13)}$$

The appropriate linear combinations $\Phi_n{}^\sigma$ and Φ_n for these branches are given in Table VI. In many cases, symmetry requires certain relations between the interatomic force constants. These are listed in Table VII for the first five nearest neighbors.

APPENDIX B

The irreducible 1/48 of the Brillouin zone (BZ) is taken to be defined by the 4 planes $\zeta_1=0.5$, $\zeta_3=0$, $\zeta_1=\zeta_2$, and $\zeta_2=\zeta_3$. [ζ_i are Cartesian coordinates of the wave vector $a\mathbf{q}/2\pi\equiv(\zeta_1,\zeta_2,\zeta_3)$.] In the present calculation, this polyhedron is subdivided into three parts labeled A, B, and C (in order of increasing ζ_1 values) by the planes $\zeta_1=1/28$ and $\zeta_1=1/14$. The normal mode frequencies are computed for wave vectors lying on a simple cubic mesh M_c of spacing $\zeta=1/252$. M_c is chosen so that the origin Γ of reciprocal space (and in fact all the corner points of BZ) lies at the body center of a basic cube of the mesh. A straightforward calculation of $g(\nu)$ on this basis would involve 341 376 matrix diagonalizations to obtain a total of 96 018 048 frequencies in the entire zone. This difficulty is avoided by diagonalizing the (6×6) dynamical matrix at points throughout the region C ($\zeta_1>1/14$) on a "crude" mesh of spacing $\zeta=1/28$. At each wave vector on this mesh (labeled X, say), the frequency gradients $\partial\nu_j/\partial\zeta_i$ are computed by standard first-order perturbation techniques[20]; the frequencies corresponding to the 729 points of the basic mesh M_c, which lie in the vicinity of each X, are then calculated by linear extrapolation from each X. These extrapolated frequencies are an excellent approximation to the "true" frequencies (which could be obtained by direct diagonalization) over most of the zone, where the frequency gradients are slowly varying. In certain regions, however, particularly for small wave vectors, this method may not be sufficiently accurate.[20] Thus we diagonalize the dynamical matrix in the region B ($1/14>\zeta_1>1/28$) on an "intermediate" mesh of spacing $\zeta=1/84$, and compute frequencies by linear extrapolation from each mesh point X for only 27 points of M_c. Finally, the region A ($\zeta_1<1/28$) is treated by diagonalization at all points M_c, without the use of perturbation theory. In total, the dynamical matrix is diagonalized at 767 different X. The distribution function $g(\nu)$ thus obtained is believed to be an extremely accurate representation of the interatomic force model $4E$ (see Sec. 3), and is adequate for the computation of all thermodynamic quantities except those that are sensitive to the moments M_n of $g(\nu)$ for which $n\leqslant-2$. In order to increase the accuracy of $g(\nu)$ for very low frequencies a second calculation was made for the regions A and B ($\zeta_1<1/14$) of BZ. The spacing of the basic mesh M_c was reduced by a factor 4 to $\zeta=1/1008$, and a three-stage system of calculation employed, similar to that described above for the full BZ. The results shown in Figs. 6 and 7 are based on a properly normalized combination of the two distributions. All the computations were performed on the Control Data G-20 computer at Chalk River.